

1998

# Second kind predictability in climate models

Chu, Peter C.

Chu, P.C., S.H. Lu, and Y. Chen, 1998: Second kind predictability in climate models. Ninth Conference on Global Change, American Meteorological Society, 86-90

http://hdl.handle.net/10945/36236

5.6

# Second Kind Predictability in Climate Models

Peter C. Chu, Shihua Lu, and Yuchun Chen
Department of Oceanography, Naval Postgraduate School, Monterey, CA 93943

## 1 Introduction

Atmospheric and oceanic numerical models are usually initial-value and/or boundary-value problems. Consider a simple one dimensional case,

$$Lu = F \tag{1}$$

with given initial condition $u(z,0)$ and boundary conditions $\partial u(z_1,t)/\partial t$ and $\partial u(z_2,t)/\partial t$. Here $u$ is velocity in $x$-direction, $k$ is vertical diffusion coefficient, $F$ includes advection, Coriolis force, and pressure gradient force, and

$$L \equiv k\frac{\partial^2}{\partial z^2} - \frac{\partial}{\partial t}$$

is a second-order differential operator. Using Green function $G$, the integral form of (1) is written as

$$u(z,t) = -\int_{z_1}^{z_2}\int_0^t G(z_0,t_0;z,t)F(z_0,t_0)dz_0dt_0$$

$$+\int_{z_1}^{z_2} u(z_0,0)G(z_0,0;z,t)dz_0 + \int_0^t \left[G\frac{\partial u}{\partial z}\right]_{z_1}^{z_2} dt_0. \tag{2}$$

Here, the right-hand side of (2) indicate the error sources for prediction: (a) inaccurate physical processes represented by the first-term, (b) inaccurate initialization represented by the second-term (here we call the first kind predictability), (c) inaccurate boundary conditions represented by the third-term, and (d) discretization (resolution). Change in either initial or boundary condition leads to a variation of model solutions. Much of the predictability research has been done on the response of model behavior to an initial value perturbation. No effort of the predictability study has been made on the response of model behavior to a boundary value perturbation.

## 2 Surface Thermal Boundary Conditions

Statistical studies show that large-scale anomalies in the distribution of sea surface temperature (SST) in the North Pacific could interact with the regional atmospheric circulation on time scales ranging from weeks to months (e.g., Namias, 1978) and that resemblance exists between the winter SST anomalies and the regional anomalies in the atmospheric geopotential height field. Numerical modeling studies have investigated the effect of large SST anomalies on the atmospheric circulation and in turn on the surface heat and moisture budget. For example, Chervin et al. (1976) integrated the NCAR general circulation model (GCM) and found statistically significant anomalies over large regions of the Northern Hemisphere in response to SST anomalies with a maximum amplitude of 12°C. For anomalies with maximum amplitude of 4°C, the atmospheric model is insensitive to the SST anomalies.

In these previous sensitivity studies, whether observational or modeling, the SST anomalies were of recognizable scale and always treated as deterministic functions of time and space. One might ask such a question: What is the atmospheric response (or in turn the air-ocean fluxes) to stochastic and tiny SST anomalies? This problem has a great practical implication. If the air-ocean fluxes are not sensitive to small random SST change, we might use low resolution (in space and time) SST input to run atmospheric models. If the air-ocean fluxes are very sensitive to tiny and random SST anomalies, we need use high quality and high resolution SST data.

## 3 Experimental Design

### 3.1 Model Description

The model that we use in this study is the NCAR Community Climate Model Version 3 (CCM3), the most recent version of the NCAR Community Climate Model. It should be noted that CCM3 has a drastic change to the previous version, CCM2, especially due to the addition of the Biosphere- Atmosphere Transfer Scheme (BATS) documented in Dickinson et al. (1993). CCM3 still uses the spectral transform method for the dynamic equations but uses a semi-Lagrangian method for transporting water (Rasch and Williamson, 1991). The model we used here contains 18 levels in the vertical with a top at 2.917 mb, and uses spherical harmonics as horizontal basis functions with a triangular truncation at wavenumber 21 (approximately a $5.6° \times 5.6°$ transform grid).

## 3.2 Tiny Gaussian-Type SST Anomalies

The National Centers for Environmental Prediction (NCEP) is compiling an atlas containing monthly mean and anomalies of SST of global oceans. Taking the year of 1994 as an example, positive SST anomalies occupied vast areas of the Atlantic Ocean (both North and South) with anomalies of 2°C in the Gulf Stream extension just off the coast of North America, negative SST anomaly (minimum -3°C) was found in January. The SST anomaly has dipole patterns in both the Pacific Ocean (northern negative and southern positive) and the Indian Ocean (northern positive and southern negative). Anomaly reaches 1-2°C except off the west coast of North America where the maximum SST anomaly is greater than 3°C in July.

In contrast to traditional studies on atmospheric response to SST anomaly, we use a Gaussian-type random variable ($\delta T$) to represent SST anomalies. The probability distribution function is given by

$$F(\delta T) = \frac{1}{\sqrt{2\pi}\sigma} \exp\left[-\frac{(\delta T)^2}{2\sigma^2}\right] \qquad (3)$$

where $\delta T$ is a random variable with a zero mean and a standard deviation of $\sigma$. Since our interest is to see the response of atmosphere to tiny random SST anomalies, we set

$$\sigma = 0.05°\text{C} \qquad (4)$$

in this study. This value (0.05°C) is less than the current instrumentation error. We used a random number generator (FORTRAN function, Ranf) to produce random disturbances for each grid point independently with mean value of zero and standard deviation of 0.05°C. Fig.1 shows one of the SST random anomaly fields generated by such a procedure. Only the large values were indicated on the map. Due to the nature of the Gaussian-type random distribution, we find several points where the SST anomalies are 2-3 times of $\sigma$, such as 0.16°C at the South China Sea and -0.13°C in the central southern Pacific Ocean.

## 3.3 Experiments

### 3.3.1 Control Run

The initial condition used in this study is 1 September's climatology of the atmospheric and surface fields, which was provided by the NCAR Climate and Global Dynamics (CGD) Division. The surface boundary conditions were monthly sea and land surface temperatures (also obtained from NCAR CGD Division) linearly interpolated onto each time step (20 min). We integrated CCM3 for 16 months from 1 September to 31 December of the next year, and used the data between 1 January to 31 December of the second year for comparison.

### 3.3.2 Anomaly Run

After three months of the control run, we added a tiny Gaussian-type random SST anomaly with zero mean and 0.05°C standard deviation (for example as shown in Fig.1) generated by the FORTRAN random number generator applied to monthly SST data (first year December to second year December), and then interpolated into each time step. The rest of the forcing was kept the same. The model were integrated from 1 December of the first year to 31 December of the second year. We compare the air-ocean interfacial fluxes of momentum, heat, and moisture for the second year between the two runs, and call the difference between anomalous minus control runs as the anomaly response.

### 3.3.3 Root-Mean-Square Difference (RMSD)

The difference of the two runs (anomaly run minus control run) of any surface variable $\psi$ is a function of space $(x, y)$, and time $t$ ,

$$\Delta\psi(x_i, y_j, t) = \psi_a(x_i, y_j, t) - \psi_c(x_i, y_j, t).$$

where $\psi_a$ and $\psi_c$ are the variables from anomaly and control runs, respectively. We define RMSD for investigating the temporal variation of the global difference,

$$RMSD_\psi(t) = \sqrt{\frac{1}{M}\sum_i\sum_j |\Delta\psi(x_i, y_j, t)|^2} \qquad (5)$$

where $M$ is the total number of horizontal grid points.

# 4 Statistical Test

The simulated fields in the two cases were analyzed in terms of monthly mean fields (near 30-day), from the second year January to December. The effect of tiny random SST anomaly on surface fluxes is presented by the difference between the two runs at each grid point. For statistical significance testing purposes, a normalized response is constructed using the procedures and estimates of the model's inherent variability from Chervin and Schneider (1976). That is, for each grid point of CCM3 a normalized response

$$r(x, y, t) = \frac{|\Delta\psi(x, y, t)|}{S_\psi(x, y, t)} \qquad (6)$$

is calculated for any variable (i.e., the tiny-random change response) at the grid point $(x, y)$ and time period $t$, and $S_\psi(x, y, t)$ is the estimate of the standard deviation of monthly averages of the variable for the CCM3 control integration. This parameter, $r$, is proportional to $t$-statistic. It allows a potential assessment of the statistical significance of the change in model behavior,

| r | Significance level for two-sided t-test |
|---|---|
| 1 | 0.5169 |
| 2 | 0.2286 |
| 3 | 0.1002 |
| 4 | 0.0469 |
| 5 | 0.0238 |
| 6 | 0.0131 |
| 7 | 0.0077 |
| 8 | 0.0047 |
| 9 | 0.0031 |

**Table 1. Significance levels for a selection of values of r corresponding to four degrees of freedom and t=r/sqrt(2) (from Chervin, 1976).**

in this case, to a tiny random SST anomaly (Chervin et al., 1980.) Chervin and Schneider (1976) had shown that the sample value of $t$ equals $r/\sqrt{2}$ at each grid point and there are four degrees of freedom. Table 1 (from Chervin, 1976) shows the relationship between $r$ and the significant level for two-sided $t$-tests. The use of the two-sided $t$-test is based on the hypothesis that there is no specific signed difference, either positive or negative, in the response to the random SST anomaly. We begin with the usual null hypothesis that the means of the two runs are equal. The significance level is the probability that the given value of $r$ is exceeded purely by chance. Equivalently , it is the probability of incorrectly rejecting the null hypothesis. As pointed by Chervin et al. (1980), we can regard as significant those response patterns which are associated with extensive regions where $r \geq 4$ (*a priori* significance criterion.) For clarity, in subsequent figures of surface flux response, we present the corresponding geographical distribution of $r$-values.

Since the added SST anomaly is a random variable, it is very hard to explain at the moment why there is strong surface flux response in certain areas. Therefore, in the subsequent sections we are concentrated more in describing the response.

# 5 Global Responses to Tiny SST Anomaly

## 5.1 Surface Wind Stress

RMSD defined by (3) is a **measure of the global response** due to SST anomalies. The temporal variation of $\mathrm{RMSD}_{\tau_x}$ (Fig.4a) and $\mathrm{RMSD}_{\tau_y}$ (Fig.4b) were computed using (3). Two modes were found from Fig.2: (a) near-linearly growing mode and (b) oscillatory mode. During the near-linearly growing mode, $\mathrm{RMSD}_{\tau_x}$ increases from 0 to near 0.2 dyne/cm$^2$ at a time scale of around 20 days, and then oscillates around this high value (0.2 dyne/cm$^2$.) between 0.24 dyne/cm$^2$ (maximum value) and 0.16 dyne/cm$^2$ (minimum value.)

During the near-linearly growing mode, $\mathrm{RMSD}_{\tau_y}$ also increases from 0 to near 0.2 dyne/cm$^2$ at a time scale of around 30 days, and then oscillates around this high value between 0.22 dyne/cm$^2$ (maximum value) and 0.16 dyne/cm$^2$ (minimum value.) except for a largest value (0.26 dyne/cm$^2$) near 260 day since the first introduced the random SST anomalies.

## 5.2 Surface Heat Budget

Temporal variation of RMSD (measure of the global response) for various surface heat fluxes also shows bimodal structure (Fig.3): (a) near-linearly growing mode and (b) oscillatory mode. During the near-linearly growing modes, the RMSDs increases from 0 to evident values at around the 20-th day:

$$RMSD_{R_S} \simeq 70W/m^2, \quad RMSD_{R_L} \simeq 42W/m^2,$$
$$RMSD_{H_S} \simeq 43W/m^2, \quad RMSD_{R_L} \simeq 76W/m.$$

During the oscillatory modes, $\mathrm{RMSD}_{R_S}$ oscillates between 76 W/m$^2$ and 49 W/m$^2$; $\mathrm{RMSD}_{R_L}$ oscillates between 43 W/m$^2$ and 33 W/m$^2$; $\mathrm{RMSD}_{H_S}$ oscillates between 50 W/m$^2$ and 32 W/m$^2$; and $\mathrm{RMSD}_{H_L}$ oscillates between 81 W/m$^2$ and 50 W/m$^2$.

## 5.3 Surface Moisture Flux

Temporal variation of RMSD for the net surface moisture flux also shows bi-modal structure (Fig.4): (a) near-linearly growing mode and (b) oscillatory mode. During the near-linearly growing modes, $\mathrm{RMSD}_{M_{net}}$ increases from 0 to an evident value (5.7 mm/day) at around the 20-th day.

During the oscillatory modes, $\mathrm{RMSD}_{M_{net}}$ oscillates between 6.8 mm/day and 4.4 mm/day.

# 6 Conclusions

1. This study shows large responses of surface fluxes to a tiny Gaussian-type random SST disturbance. It is quite surprising that the responses of surface fluxes were very strong, even in the monthly mean values. It might lead to a second kind of unpredictability caused by some uncertainty in the boundary conditions.

2. Two modes of the global response were found in this study: (a) near-linearly growing mode and (b) oscillatory mode. During the near-linearly growing modes, the **difference of the root-mean-squares** (RMSDs) increase from 0 to evident values at around the 20-th day:

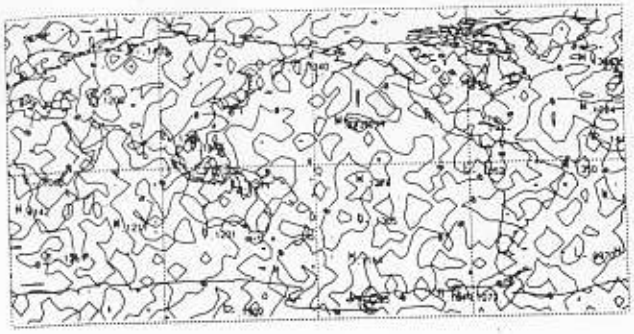

Figure 1 – One set of SST random anomaly with mean of zero and standard deviation of 0.05 degree C.

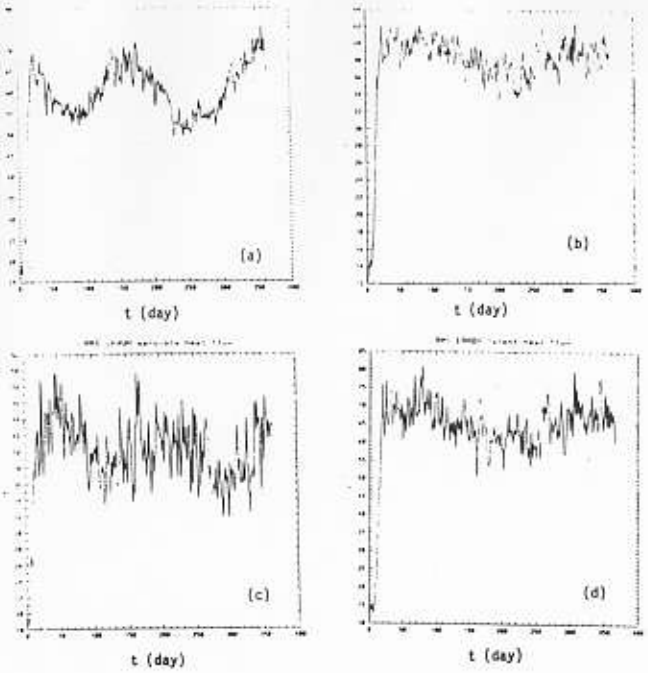


Figure 3 – Temporal RMSD variation of the various surface heat fluxes ($W/m^2$): (a) solar radiation, (b) long-wave radiation, (c) sensible heat flux, (d) latent heat flux. The horizontal axis t=0 indicates the first day when the tiny random SST anomaly was in

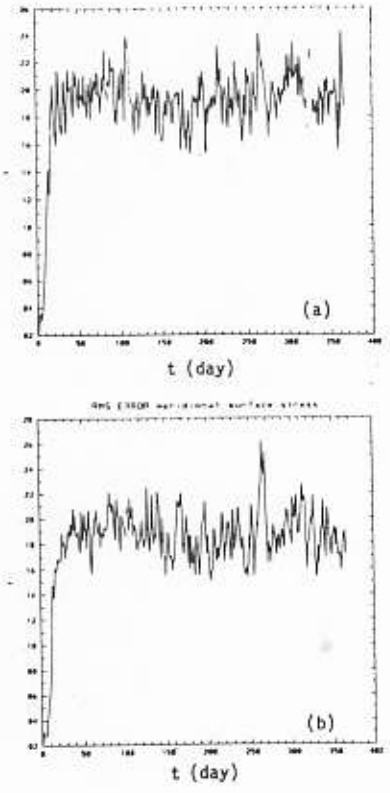


Figure 2 – Temporal RMSD variation of the surface wind stresses (dyne/$cm^2$ ): (a) zonal component, and (b) latitudinal component. The horizontal axis t=0 indicates the first day when the tiny random SST anomaly field is added.

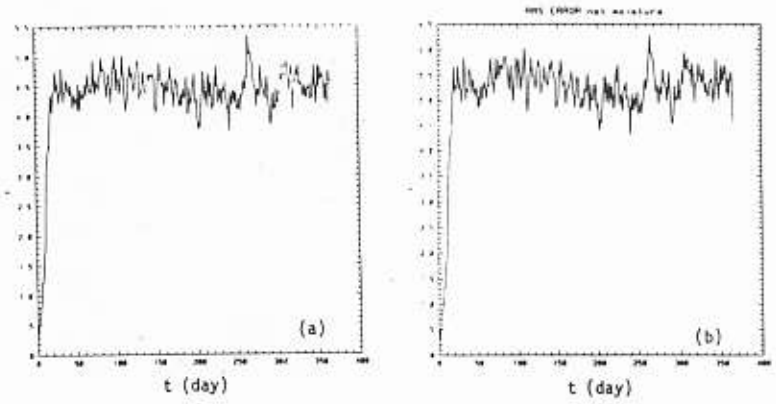


Figure 4 – Temporal RMSD variations of the various surface moisture fluxes (unit: mm/day ): (a) precipitation, and (b) net surface moisture flux. The horizontal axis starts from the first day (t=0) when the tiny random SST anomaly was introduced.

$$RMSD_{R_S} \simeq 70W/m^2, \quad RMSD_{R_L} \simeq 42W/m^2,$$
$$RMSD_{H_S} \simeq 43W/m^2, \quad RMSD_{R_L} \simeq 76W/m,$$
$$RMSD_{\tau_x} \simeq 0.2dyne/cm^2, RMSD_{\tau_y} \simeq 0.2dyne/cm^2$$
$$RMSD_{M_{net}} \simeq 5.7mm/day$$

During the oscillatory modes, RMSDs oscillates around these evident values.

3. Several geographic locations were found sensitive to the tiny-SST anomalies: Polar regions, Tibetan Plateau, Northeast Australia, North Africa, South tip of the Africa, and western Pacific.

4. Integration of atmospheric model needs accurate SST data. The noise in the SST data may bring drastic change in the model results.

5. From the RMSD values, we estimate that the uncertainty of 0.28 dyne/cm$^2$ in the surface wind stress, of 70 W/m$^2$ in the surface heat flux, and of 5.7 mm/day in the net moisture flux.

# 7 ACKNOWLEDGMENTS

This research was sponsored by the Office of Naval Research (ONR) NOMP Program, Naval Oceanographic Office, and the Naval Postgraduate School.

# REFERENCES

Bourke, W., B. McAvanney, K. Puri, and R. Thurling, Global modeling of atmospheric flow by spectral methods, **Methods in Computational Physics,** 17, General Circulation Models of the Atmosphere, J. Chang, Ed., Academic Press, 267-324, 1977.

Briegleb, B.D., Delta-Eddington approximation for solar radiation in the NCAR Community Climate Model, **J. Geophys. Res.,** 97, 7603-7612, 1992.

Chervin, R.M., W.M. Washington and S.H. Schneider, Testing the statistical significance of the response of the NCAR general circulation model to North Pacific Ocean surface temperature anomalies, **J. Atmos. Sci.,** 33, 413-423, 1976.

Chervin, R.M., J.E. Kutzbach, D.D. Houghton and R.G. Gallimore, Response of the NCAR general circulation model to prescribed changes in ocean surface temperature. Part II: Midlatitude and subtropical changes, **J. Atmos. Sci.,** 37, 308-332, 1980.

Davis, R.E., Predictability of sea surface temperature and sea level pressure anomalies over the North Pacific Ocean, **J. Phys. Oceanogr.,** 6, 249-266, 1976

Dickinson R.E., A. Herderson-Sellers, and P.J. Kennedy, Biosphere-Atmosphere Transfer Scheme (BATS) Version 1e as coupled to the NCAR Community Climate Model, **NCAR Technical Note,** 1993.

Douglas, A.V., D.R. Cayan, and J. Namias, Large-scale changes in North Pacific and North American weather patterns in recent decades, **Mon. Wea. Rev.,** 110, 1851-1862, 1982.

Hack, J.J., B.A. Boville, B.P. Briegleb, J.T. Kiehl, P.J. Rasch, and D.L. Williamson, Description of the NCAR Community Climate Model (CCM2), **NCAR Technical Note,** NCAR/TN-382+STR, 1993.

Holtslag, E.I., F. de Bruijn, and H.-L. Pan, A high resolution air mass transformation model for short-range weather forecasting. **Mon. Wea. Rev.,** 118, 1561-1575, 1990.

Kiehl, J.T., Modeling and validation of clouds and radiation in the NCAR Community Climate Model, **Proc. ECMWF/WCRP Workshop on Clouds, Radiative Transfer and Hydrological Cycle,** 413-450, Reading, 12-15 November 1990.

Kutzbach, J.E., R.M. Chervin and D.D. Houghton, Response of the NCAR general circulation model to prescribed changes in ocean surface temperature Part I: Mid-latitude changes, **J. Atmos. Sci.,** 34, 1200-1213, 1977.

McAvaney, B.J., W. Bourke and K. Puri, A global spectral model for simulation of the general circulation, **J. Atmos. Sci.,** 35, 1557-1583, 1978.

Namias, J., Multiple causes of the North American abnormal winter 1976-77, **Mon. Wea. Rev.,** 106, 279-295, 1978.

NCEP, **Climate Diagnostics Bulletins,** Climate Prediction Center, 1995

Ramanathan, V., E.J. Pitcher, R.C., Malone and M.L. Blackmon, The response of a spectral general circulation model to refinements in radiative processes, **J. Atmos. Sci.,** 40, 605-630, 1983.

Rasch, P.J. and D.L. Williamson, The sensitivity of a general circulation model climate to the moisture transport formulation, **J. Geophys. Res.,** 96, 13,123-13,137, 1991.

Slingo, A., A GCM parameterization for the shortwave radiative properties of water clouds, **J. Atmos. Sci.,** 46, 1419-1427, 1989.